Thin Solid Films 745 (2022) 139103

Contents lists available at ScienceDirect

Thin Solid Films

journal homepage: www.elsevier.com/locate/tsf

Influence of molecular weight of polycation polydimethyldiallylammonium and carbon nanotube content on electric conductivity of layer-by-layer films

Sven Neuber [a], Annekatrin Sill [a], Ilias Efthimiopoulos [a], Peter Nestler [b], Katja Fricke [c], Christiane A. Helm [a,*]

[a] Institute of Physics, University of Greifswald, Felix-Hausdorff-Straße 6, D-17489 Greifswald, Germany
[b] ZIK-HIKE - Biomechanics, University of Greifswald, Fleischmannstr. 42, D-17489, Germany
[c] Leibniz Institute for Plasma Science and Technology, Felix-Hausdorff-Straße 2, D-17489 Greifswald, Germany

A B S T R A C T

For biological and engineering applications, nm-thin films with high electrical conductivity and tunable sheet resistance are desirable. Multilayers of polydimethyldiallylammonium chloride (PDADMA) with two different molecular weights (322 and 44.3 kDa) and oxidized carbon nanotubes (CNTs) were constructed using the layer-by-layer technique. The surface coverage of the CNTs was monitored with a selected visible near infrared absorption peak. Both the film thickness and the surface coverage of the CNTs increased linearly with the number of CNT/PDADMA bilayers deposited (film thickness up to 80 nm). Atomic force microscopy images showed a predominantly surface-parallel orientation of CNTs. Ohmic behavior with constant electrical conductivity of each CNT/PDADMA film and conductivity up to $4 \cdot 10^3$ S/m was found. A change in PDADMA molecular weight by almost a factor of ten has no effect on the film thickness and electrical conductivity, only the film/air roughness is reduced. However, increasing CNT concentration in the deposition dispersion from 0.15 up to 0.25 mg/ml results in an increased thickness of a CNT/PDADMA bilayer (by a factor of three). The increased bilayer thickness is accompanied by a decreased electrical conductivity (by a factor of four). The decreased conductivity is attributed to the increased monomer/CNT ratio.

1. Introduction

Electrically active implants are often isolators covered by an electrically conducting coating [1,2]. Ultrathin organic films as coatings were investigated. For applications, the sheet resistance R_s of the coating needs to be low and adjustable. For very thin films to be sufficient, high electrical conductivity is required [3–7]. One way to reduce the sheet resistance of an organic film is to make a composite material with electrically conductive carbon nanotubes (CNTs). Electrically conductive films of carbon nanotubes have been made many different ways. However, the influence of film composition on electrical conductivity is far from clear. We used the layer-by-layer (LbL) technique and found constant electrical conductivity above a certain number of layers. With constant electrical conductivity, it is possible to tune the sheet resistance within an order of magnitude by adjusting (i) the preparation conditions and (ii) the thickness of the film.

In the LbL technique, films are prepared by the consecutive adsorption of oppositely charged polyions [8–11]. The film thickness can be controlled by the number of deposition steps. To identify the composition of the film, absorption spectra of one component can be used. At first glance, the visible and near infrared (Vis-NIR) absorption spectrum of CNTs is complicated [12]: Depending on the preparation of CNTs different absorption spectra are observed, and the correlation between CNT absorption spectrum and other physical properties of CNTs is not yet established. However, we find that for a specific preparation procedure typical absorption peaks can be identified.

Kotov and coworkers [13] showed that it is possible to form electrically conductive LbL films by using polyelectrolytes (PE) and CNTs. CNTs have interesting electrical properties: Due to freely moving electrons, the electrical conductivity of a multi-walled carbon nanotube can be large ($\sim 10^7$ S/m) [14]. Therefore, we use multi-walled nanotubes. However, even for μm-thick films consisting of CNTs only, the conductivity is reduced by a factor of 10 to 100 (up to $6.7 \cdot 10^5$ S/m) [15,16]. Between CNTs, electrons are transferred by a hopping process between touching CNTs. Compared to a single nanotube, the charge transfer between CNTs reduced the conductivty of that film by one to two orders of magnitude [3,4]. Multilayers consisting only of organic polyelectrolytes have a low elelctrically conductivity; it is fourteen to sixteen

* Corresponding author.
E-mail address: helm@uni-greifswald.de (C.A. Helm).

https://doi.org/10.1016/j.tsf.2022.139103
Received 2 August 2021; Received in revised form 8 January 2022; Accepted 17 January 2022
Available online 20 January 2022

orders of magnitude smaller than that of a CNT, 10^{-9} S/m to 10^{-7} S /m; conductivity occurs by ion transport [17]. Therefore, high electrical conductivity in LbL films can only be achieved by CNTs which touch at cross-over points and allow the electrons to hop from one CNT to the next.

For LbL film assembly, the dispersion of hydrophobic CNTs in water is necessary. In the past, this was achieved by chemically modifying the CNTs with functional groups or by wrapping them in polyanions, usually poly(styrenesulfonate sodium salt) (PSS) [18,19]. LbL films prepared from two kinds of chemically modified CNTs (one kind of CNT was positively charged, the other negatively) showed a low conductivity (200 S/m to 800 S/m), three orders of magnitude lower than found in films prepared of pure CNTs [20]. LbL films made from single-wall CNTs wrapped in PSS and a second polyelectrolyte exhibited a somewhat larger conductivity: 430 S/m with CNTs and laminin [13] or 1000 S /m with CNTs and polyvinyl alcohol [18]. We shall show that oxidation of the CNTs and close packing leads to a larger conductivity.

To complement the Vis-NIR absorption measurements, the film surface is imaged by atomic force microscopy (AFM) and the film thickness is determined by ellipsometry. We modified the CNTs (single-walled/double-walled mixture; carbon nanotubes ratio > 90%, diameter 1 to 2 nm, length 5 to 30 μm) by chemical oxidation to obtain negatively charged CNTs. To achieve a high packing density of the film, a strong linear polycation (polydimethyldiallylammonium chloride, PDADMA) was used. To adjust the CNT surface coverage per deposition step, the CNT concentration in the dispersion was varied. To influence the thickness per polycation adsorption layer, the molecular weight of PDADMA was varied by almost a factor of ten [21].

2. Materials and methods

2.1. Chemical modification of CNTs

To obtain negatively charged CNTs, they were treated with a mixture of concentrated acid. This process is necessary to reduce the hydrophobicity of the CNT sidewalls and thus, to increase the dispersion of the CNTs in water. The acid treatment presumably leads to the formation of holes and oxidative etching along the walls of the CNTs [22–24]. The acid mixture of concentrated H_2SO_4 and HNO_3 produces electrophilic groups like NO_2^+, which can attack the -C = C- double bonds. This creates new defects. In addition, the H_2SO_4 molecule can attack the created and existing defect sites. A C-OSO_2OH bond is formed which, when reacted with water, leads to a-OH bond [25].

Hydrophobic CNTs (512 mg, single-walled/double-walled mixture; CNT ratio > 90%, diameter 1 to 2 nm, length 5 to 30 μm, abcr GmbH, Karlsruhe, Germany) were treated with 50 ml of a volume/volume ratio (1:3) of a HNO_3 (60–68%)/H_2SO_4 (98%) acid mixture at 80 °C for 3.5 h according to the procedure proposed by López-Oyama [22].

The obtained dispersion was filtered under vacuum and washed with deionized water until the pH of the rinsing water became neutral. The solvent was removed with the use of a liquid nitrogen rotary evaporator and modified CNTs were dried overnight via lyophilization. After the chemical treatment, 65 mg of dry CNTs were obtained (at ambient conditions), due to addition of some negative charges. This allowed the CNTs to be used as polyanions. For a fine dispersion in water, raw CNTs were put in a solution containing 2 wt% sodium dodecyl sulfate (SDS), purchased from Carl Roth GmbH+Co. KG, Karlsruhe, Germany.

2.2. Film preparation

Single side polished silica wafer (Silicon Materials, Kaufering, Germany) and microscope slides (76 mm × 26 mm, Carl Roth GmbH + Co. KG, Karlsruhe, Germany) were cleaned according to a RCA treatment protocol [26] and used as substrate. The polyelectrolyte multilayers in combination with freshly modified CNTs were prepared by the LbL-method [27], sequential adsorption of oppositely charged PEs and CNTs from solution with the help of a dipping robot (Riegler & Kirstein GmbH, Potsdam, Germany) and a refrigerated circulation thermostat (Carl Roth GmbH + Co. KG, Karlsruhe, Germany) at 20 °C.

As polycations poly(ethylenimine) (PEI, branched, M_w = 750kDa, PDI = 12.5) and PDADMA (M_w = 44.3kDa and 322kDa, PDI = 2.19) were used. As polyanions we used PSS (M_w = 666kDa, PDI < 1.2) and modified CNTs. PEI was purchased from Sigma Aldrich Chemie GmbH (Steinheim, Germany), PDADMA and PSS from Polymer Standards Service (Mainz, Germany). For the polyelectrolyte solutions, the composition of the adsorption solution was 1 mM PE with respect to the monomer concentration solved in 100 mM NaCl (Merck KGaA, Darmstadt, Germany). The modified CNT concentration was 0.15 mg/ml and 0.25 mg/ml suspended in ultrapure water. The adsorption time for each deposition step was 30 min with three subsequent washing steps (each step 1 min) with ultrapure water (nominal conductivity of 0.054 μS/cm, Sartorius arium advance, Göttingen, Germany, followed by Millipore purification system, Molsheim, France) to remove the loosely bond polycations or polyanions. For all films the first adsorbed layer was PEI followed by a PSS layer. Then the PDADMA and the CNTs were absorbed in an alternating sequence. Therefore, the overall film structure is PEI/PSS/PDADMA/$(CNT/PDADMA)_N$, abbreviated as CNT/PDADMA film.

2.3. Atomic force microscopy

Surface morphology was determined with a DI Multimode AFM using NanoScope IIIa software from Veeco (Santa Barbara, CA, USA). As cantilever a RTESP-300 model (BRUKER, Billerica, MA, USA) was used with a tip radius < 10 nm. All measurements were done in the AFM tapping mode with dry samples at ambient conditions. At least 3 different positions of each sample were imaged with a scan size of 5 μm × 5 μm. For data analysis, the NanoScope Analysis (version 1.90, 32 bit) software from BRUKER (Billerica, MA, USA) was used. Beside imaging AFM is also used to quantify sample surface roughness, which is calculated via root mean square (RMS) deviation from measured height profiles.

AFM scratch images for comparison with ellipsometric measurements were recorded with JPK NanoWizzard 3 (JPK Instruments, Berlin, Germany) using OMCL-AC160TS cantilever (Oxford Instruments, Wiesbaden, Germany) with measured spring constant 61.8 N/m and sensitivity 29.7 nm/V.

2.4. Vis-NIR absorption spectroscopy

Vis-NIR spectra of the dry films were recorded with a Lambda 900 UV–Vis spectrometer from Perkin-Elmer (Wiesbaden, Germany), at 30% r.h.. The films were measured directly with the microscopic slides (76 mm × 26 mm, Carl Roth GmbH + Co.KG, Karlsruhe, Germany) at ambient conditions (≈ 21°C and relative humidity ≈ 30%). The slide was covered at both sides due to preparation conditions. To obtain the absorbance of one film, the obtained values were divided by two. The determination of the extinction coefficient was done with a CNT suspension in a cuvette (Rotilabo®-single-use cells, 4 ml, Carl Roth GmbH + Co. KG, Karlsruhe, Germany). According to the Beer-Lambert law the absorbance is given by $A = -\log\left(\frac{I}{I_0}\right) = \varepsilon \cdot d \cdot c$. The incident intensity is I_0 (at a particular wavelength), I is the transmitted intensity after passing through a sample with a thickness d, containing a concentration c of the absorbing species with a wavelength-dependent extinction coefficient ε. Absorption was measured from 400 nm to 1800 nm with 5 nm/s steps and an integration time of 1 s per step.

2.5. Ellipsometry

CNT/PDADMA film thickness d_{film} was determined by null-

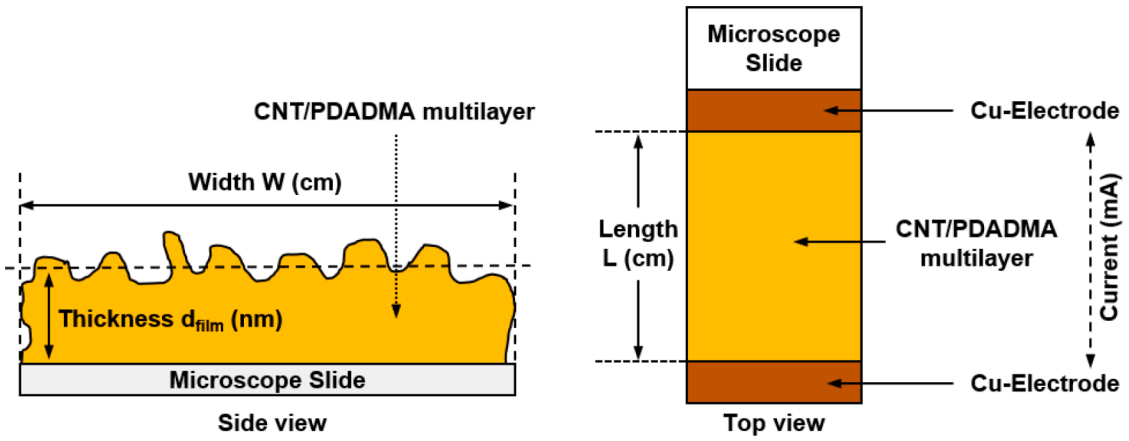

Scheme 1. Sketch of an electrically conductive film on top of a non-conductive substrate. The sheet resistance of the thin film depends on its length L, its width W and its thickness d_{film}. Here, the film consists of a carbon nanotube/polycation (CNT/PDADMA) multilayer.

ellipsometry (Multiskop, Optrel GbR, Sinzing, Germany). A He-Ne laser (power 4 mW, wavelength $\lambda = 632.8$ nm) serves as light source. A CNT/PDADMA film is described by a homogeneous film thickness as well as its complex refractive index $n_{film} - i{\cdot}\kappa_{film}$. Here, n_{film} is the real part of the refractive index, i the imaginary unit and κ_{film} is the extinction coefficient indicating the light attenuation while passing the non-transparent CNT/PDADMA film. Effects of surface roughness are neglected. By measuring the ellipsometric angles Ψ and Δ of a CNT/PDADMA film the three film parameters d_{film}, n_{film} and κ_{film} are fitted using a slab model [28]. However, determining three film parameters based on two independently measured values (Ψ and Δ) may leave the resulting values vulnerable to parameter cross-coupling. Therefore, all ellipsometric measurements were carried out at several angles of incidence (66° to 72° in 1° steps) [29]. Moreover, for each sample condition light absorption A_{film} was measured independently by Vis-NIR absorption spectroscopy (Lambda 900, Perkin-Elmer, Wiesbaden, Germany) at the wavelength 635 nm. According to Beer-Lambert law the absorption A_{film} is connected to the attenuation coefficient $\alpha = \ln(10){\cdot}A_{film}/d_{film}$ which is in turn connected to the extinction coefficient $\kappa_{film} = \alpha{\cdot}\lambda/(4\pi)$. Thus, for ellipsometric data analysis κ_{film} was always determined by the condition $\kappa_{film}(A_{film}, d_{film}) = \ln(10){\cdot}A_{film}\lambda/(4\pi{\cdot}d_{film})$ reducing the effective number of free fitting parameters to two (d_{film} and n_{film}). d_{film} is required to quantify the sheet resistance R_S. Therefore, the reliability of d_{film} determination by ellipsometry is confirmed by AFM. AFM-based thickness determination is purely mechanically and serves as an independent method to gain the film surface height distribution

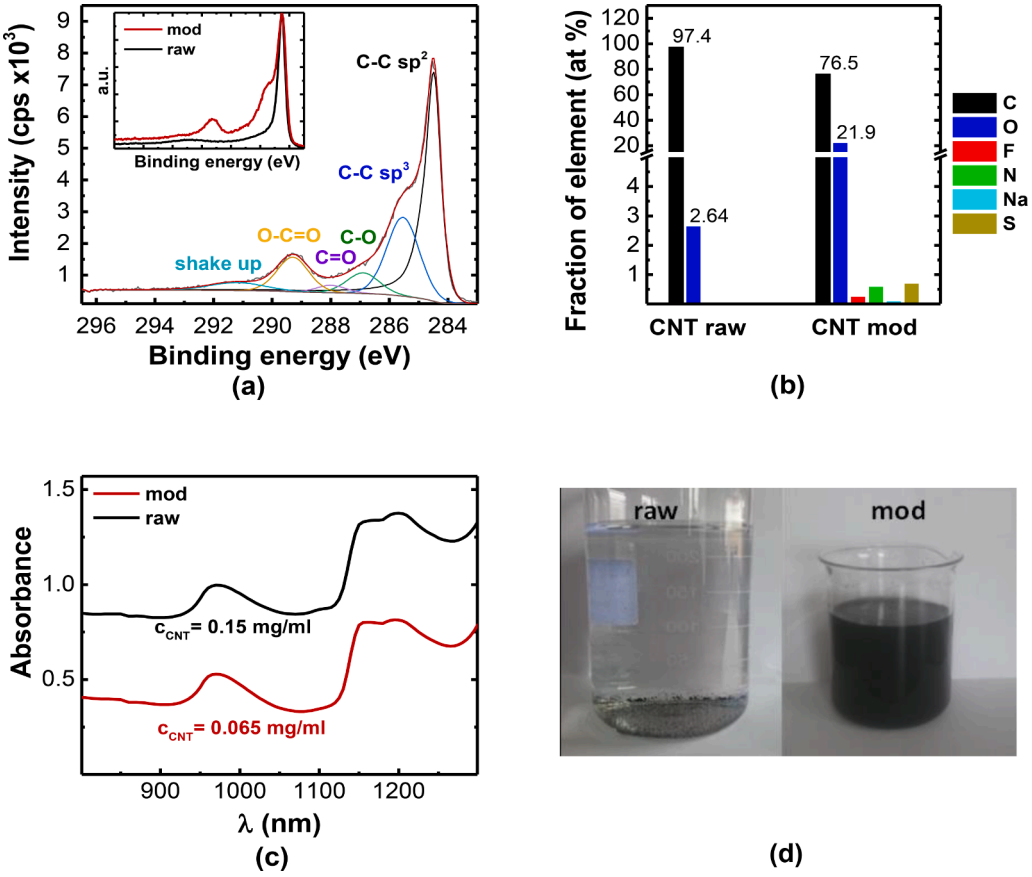

Fig. 1. Characterization of CNTs before and after acid treatment, indicated "raw" and "mod", respectively. **(a)** XPS: Peak-fit of the high-resolution C1s peak of CNT after acid treatment. Note the large fraction of C—C bonds in sp^3 hybridization. Inset: the original normalized data, both for raw (black) and modified (red) CNTs (normalized with respect to the C—C sp^2 peak). **(b)** Fraction of atoms found in XPS before and after acid treatment, as indicated. **(c)** Optical absorption data of CNTs dissolved in water before and after acid treatment. CNT concentration was 0.15 mg/ml (before treatment, and 2 wt% SDS) and 0.065 mg/ml (after treatment). Note the absorption peak at 970 nm. **(d)** CNT dispersion before (raw, without SDS) and after (mod) modification.

relative to the substrate. Ellipsometry derived film thickness (with neglected roughness) matches the mean value of the surface height distribution within 1 nm error.

2.6. Electrical conductivity

Electrical properties of CNT/PDADMA films at ambient conditions (10% to 15% r.h.) were measured with an ELNEOS FIVE multimeter (Ernst Fischer GmbH + Co.KG, Freudenstadt, Germany). The device includes a waveform generator and a digital ampere– and voltmeter. The set-up is shown in Scheme 1: a glass slide is covered by an electrically conductive film. Measured is the ohmic resistance $R = \frac{U}{I}$ which will then be normalized to determine the sheet resistance ($R_S = \frac{1}{\sigma} \frac{L}{W \cdot d_{film}}$ with L the length, W the width, d_{film} the film thickness and σ the conductivity) [30,31]. For data analysis, the resistivity ρ is determined which is the inverse of the conductivity, $\sigma = 1/\rho$.

2.7. X-ray photoelectron spectroscopy (XPS)

Surface elemental composition was determined by high resolution scanning XPS [32,33]. Charge neutralization was implemented by low energy electrons, injected in the magnetic field of the lens from a filament located directly atop the sample. Spectra were acquired using an Axis Supra DLD electron spectrometer (Kratos Analytical, Manchester, UK) with a monochromatic Al Kα source (1486.6 eV). The instrument was set to the medium magnification lens mode and by selecting the slot mode, providing an analysis area of approximately 250 μm in diameter. Core level spectra of F1s, O1s, N1s, C1s, Na1s and S2p were collected at an analyser pass energy of 80 eV and for the highly resolved measured C1s peak the pass energy was set to 10 eV. Data acquisition and processing were carried out using Casa XPS software, version 2.3.22PR1.0 (Casa Software Ltd., Teignmouth, UK). Concentrations are given in atomic percent (at %). Curve-fitting procedure of the C1s high-resolution spectrum was performed after Shirley background subtraction to characterize the chemical structure of the surface. Peak positions of the carbon species, based on literature data [34], were: aromatic carbon (C—C sp^2, 284.5 eV), aliphatic carbon (C—C sp^3, 285.5 eV), hydroxyl (C—OH, 286.9 eV), epoxy (C—OC, 286.9 eV), carbonyl (C═O, 288.0 eV) and carboxyl (O—C═O, 289.3 eV). The full width at half maximum of the C1s components was 0.5 eV to 1.3 eV for high energy resolution measurements.

3. Results and discussion

3.1. X-ray photoelectron spectroscopy

XPS measurements were performed to obtain information on the chemical composition and the nature of chemical bonds of the CNTs. The peak fit of the high-resolution C1s XPS spectra of untreated and chemically modified CNTs are shown in Fig. 1(a). Changes in the peak shape of the modified CNT show that a lot of oxygen has been bound to the surface of the CNT. The C1s spectrum of the untreated CNTs is characterized by a main peak at 284.5 eV with an asymmetric shape attributed to graphitic carbon sp^2. Also, a π-π* satellite peak at a binding energy of 288 eV to 294 eV is observed, typical for CNTs [35–37]. Amorphous carbon is expected within 284.5 eV to 284.7 eV, indicating mainly sp^3 hybridization, carbon with sp^2 hybridization and defect sites in a non-aromatic form [38]. The C1s spectrum of the modified sample were fitted with 6 peaks (cf. Fig. 1(a)) at binding energies of 284.5 eV, 285.5 eV, 286.9 eV, 288 eV, 289.3 eV and 291 eV, respectively. Again, the main peak at 284.5 eV corresponds to graphitic carbon sp^2. The peaks at 286.9 eV, 288 eV and 289.3 eV correspond to three different oxygen-containing environments, in particular C—O, C═O and O—C═O. The position of the peaks is expected since strong and covalent bonds of oxidative carbon lead to lower electron densities at the carbon atom, which lead to positive chemical shifts (286.1 eV to 291 eV). The elemental surface composition of CNT before and after acid treatment is shown in Fig. 1(b).

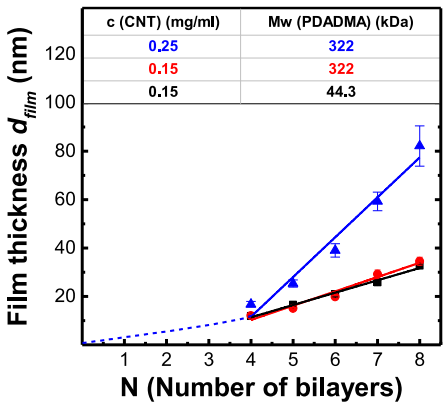

Fig. 2. PEI/PSS/PDADMA/(CNT/PDADMA)$_N$ films, with N the number of CNT/PDADMA BL. Varied was the molecular weight of the polycation PDADMA and the concentration of the CNTs in the adsorption solution as indicated. The measurements were performed in air with ellipsometry. PDADMA, PSS and PEI were adsorbed from 0.1 M NaCl solution. All thicknesses are average values determined from three different films. The error bars indicate the standard deviation.

After the treatment an increase of the oxygen content from 2.6 at.% to 21.9 at.% was determined. Furthermore, contaminations of F, Si and Na originating from the wet chemical process were detected by XPS. Even if every C atom is oxidized at the exposed ends of the CNTs, this would correspond to a much lower oxygen percentage than observed (cf. Fig. 1(b)).

Based on the XPS results, the majority of the oxygen atoms must be bound to the defective sites on the CNT sidewalls [23,24]. The acidic oxidative treatment of the CNTs can change its structural properties considerably. Note that the peak at 291 eV (cf. Fig. 1(a)) corresponding to the π-π* shake-up transition is reduced considerably after treatment, indicating a disturbance of the π electron system and thus to a change in the electronic structure of the CNT side walls [23].

Additionally, the defects on the CNT structure have increased dramatically compared to the untreated sample (at 285.5 eV) [38–41]. Therefore, we assume that not only an oxidative attack on existing carbon defect sites occurred, but also CNTs were shortened and additional defects were generated, which could be further oxidized [38]. In summary XPS data revealed that the acid treatment introduced hydroxyl, aldehyde and carboxyl groups, all of them hydrophilic and weakly negatively charged in water ($pH_{\text{modified CNTs in water}} = 3.8$).

3.2. Absorption in solution

Absorption measurements in the near IR (cf. Fig. 1(c)) of fine dispersed raw CNT in aqueous solution (with the help of SDS) show two peaks; one at ≈ 970 nm and the other at ≈ 1140 nm. These peaks are related to large-diameter single-walled and/or double-walled CNTs [12]. Interestingly, the acid treatment causing the addition of negatively charged groups renders the CNTs and allowed a fine dispersion in water (cf. Fig. 1(d)), yet the peaks attributed to the delocalized π-electrons and the CNTs remain the same.

From the absorption spectrum of CNTs in solution (cf Fig. 1(c)), the extinction coefficient ε was calculated ($\varepsilon \approx 8\ l\ g^{-1}cm^{-1}$ at 970nm). Therefore, the CNTs can now be described as polyanions. They were integrated in the LbL preparation process instead of classical polyanions like PSS.

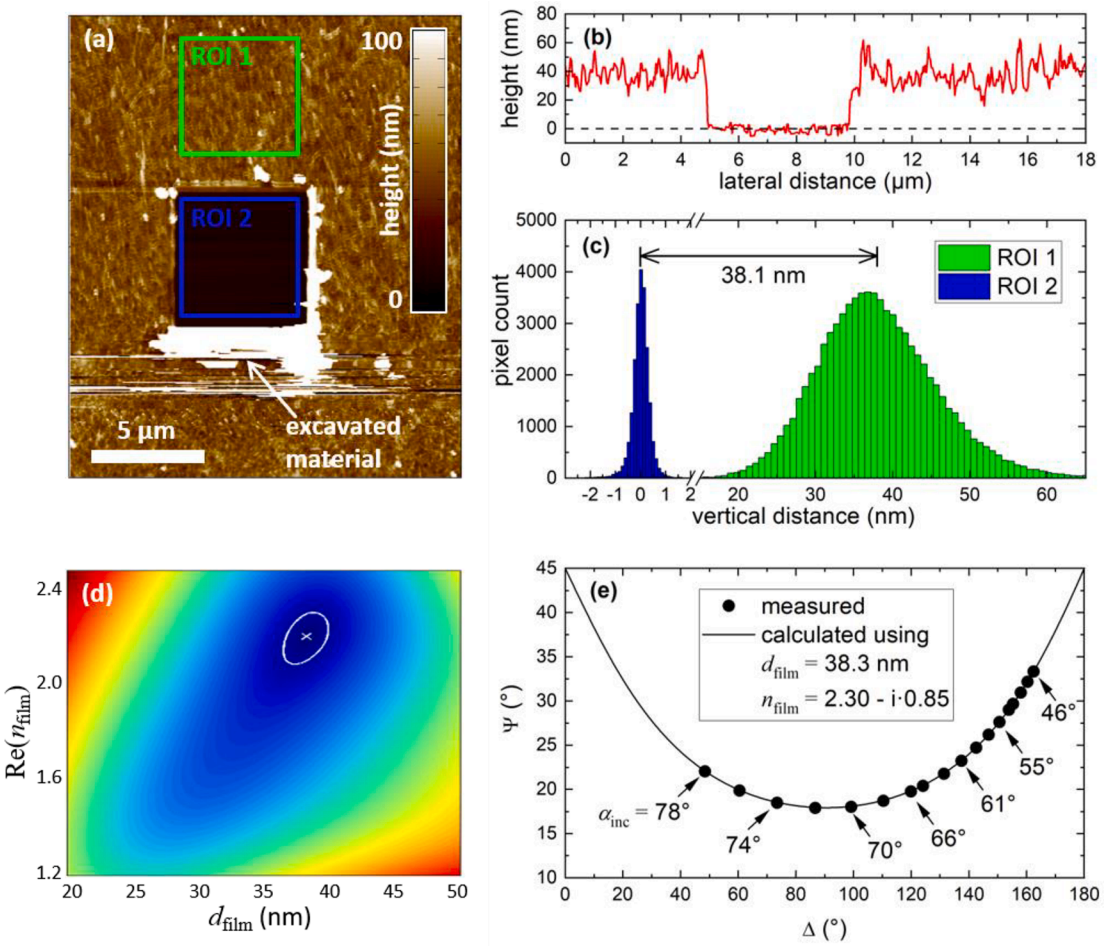

Fig. 3. Comparison of AFM-based and ellipsometric thickness determination. **(a)** AFM tapping mode image of PDADMA/CNT multilayer film (8 bilayers, $M_{w,PDADMA}$ = 44.3 kDa) treated by the AFM 'furrow method' [42]. Prior to imaging in AFM tapping mode, a 6 µm × 6 µm subarea was scanned several times in AFM contact mode with a vertical force of 1.5 µN (region of interest ROI 2, blue frame). The contact force is sufficient to displace the multilayer material, but too low to damage the underlying Si substrate. The ROI 1 region (green frame) is a typical multilayer region that is not affected by the contact mode process (scratching). **(b)** Exemplary sample height profile along a section line through the trench region ROI 2 shown in (a). **(c)** Histograms of the height distributions of ROI 1 and ROI 2, respectively, as depicted in (a). The root mean square (RMS) roughness within the trench (ROI 2) is about 1 nm, as is typical for a bare Si wafer, suggesting complete multilayer ablation. In contrast, ROI 1 is characterized by an RMS roughness of 8 nm and a mean height of 38.1 nm. This value deviates slightly from the distribution peak (at 36.8 nm) due to the skewness of the height distribution. **(d)** Color-coded least mean squared residuum of the ellipsometric fitting procedure. Systematic variation of the fitting parameters d_{film} and $Re(n_{film})$ results either in good agreement (dark blue region) or significant discrepancy (red and yellow regions) with the experimental ellipsometric data. The best agreement is indicated by a white cross (d_{film} = 38.3nm and $Re(n_{film})$ = 2.30) and the closed white line indicates the confidence interval of the parameters. The sample studied is the same as shown in (a)-(c). **(e)** Measured ellipsometric angles Δ and Ψ at various angles of incidence α_{inc} (black circles) and the calculated trajectory (black line) determined by least square regression as shown in (d).

3.3. Film deposition monitored by ellipsometry

The film growth of CNT/PDADMA multilayers was monitored with null-ellipsometry, in air at ambient conditions (cf. Fig. 2) [28,29]. All measurements were obtained from three films of the same structure, each built under the same conditions. Averages of these measurements are shown. In order to verify the thickness measured by ellipsometry we compared the results with AFM measurements as a cross check (cf. Fig. 3). For all films studied, the thickness of the first three CNT/PDADMA bilayers (BL) did grow non-linearly with the number N of deposited BL. Varied was the molecular weight of PDADMA and the concentration of the CNTs in the deposition solution.

Starting at four bilayers, the film thickness increased linearly with the number of deposited CNT/PDADMA BL (cf. Fig. 2). Films which were produced with a high CNT concentration of 0.25mg/ml were the thickest, those with a concentration of 0.15mg/ml CNTs were the thinnest. The variation of the PDADMA molecular weight from 322kDa down to 44.3kDa did not have any significant effect on the film growth, respectively thickness. The thickness for each deposited CNT/PDADMA BL prepared with a CNT concentration of 0.15mg/ml is (5.5 ± 0.5) nm, independent of the PDADMA molecular weight (to be exact: (5.9 ± 0.6) nm for $M_{w,PDADMA}$ = 322kDa and (5.1 ± 0.3) nm for $M_{w,PDADMA}$ = 44.3kDa). After increasing the CNT concentration up to 0.25mg/ml, the thickness for each deposited CNT/PDADMA BL also increased to (16.5 ± 1.7) nm, which is about a factor of three larger. All investigated films appeared stable and homogeneous.

3.4. Vis-NIR absorbance spectroscopy

Ellipsometric measurements showed that the average thickness of a deposited CNT/PDADMA BL depends on the concentration of CNTs in suspension. To find out whether the CNT coverage depends on the polycation molecular weight, the films were investigated by Vis-NIR absorbtion spectroscopy (cf. Fig. 4). The absorption spectra of individual CNT/PDADMA films show qualitatively similar single peaks at 1100nm. However, in comparison, the CNT suspension showed two

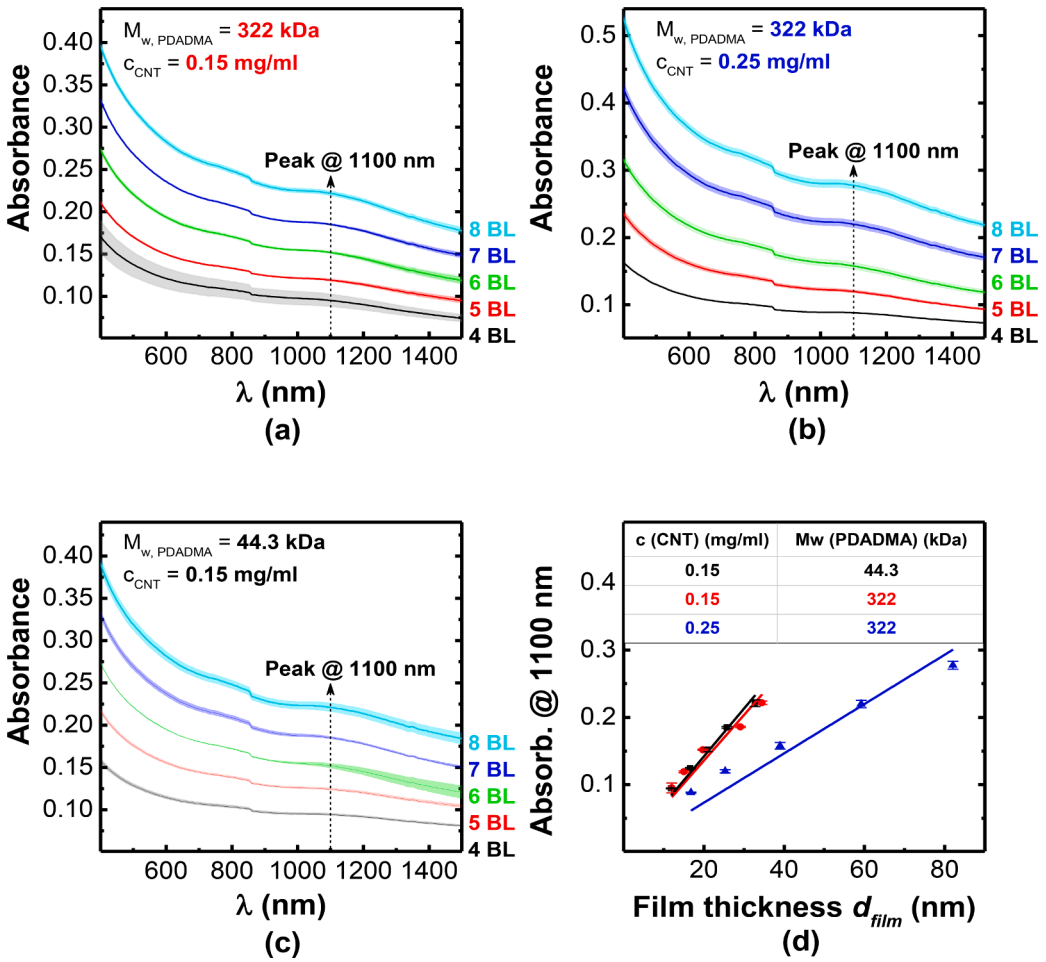

Fig. 4. Vis-NIR absorbance spectra in air of PEI/PSS/PDADMA/(CNT/PDADMA)$_N$ films in dependence of N, the number of deposited CNT/PDADMA BL. Varied is the concentration of CNTs in the adsorption dispersion and the molecular weight of PDADMA: **(a)** $M_{w,PDADMA}$ = 322kDa and c_{CNT} = 0.15mg/ml, **(b)** $M_{w,PDADMA}$ = 322kDa and c_{CNT} = 0.25mg/ml and **(c)** $M_{w,PDADMA}$ = 44.3kDa and c_{CNT} = 0.15mg/ml. **(d)** Dependence of absorbance at 1100 nm on the film thickness. All absorption measurements are the average obtained from three different films; in (d), the error bars represent the standard deviation.

distinct absorption peaks slightly above and below 1100nm, respectively (cf. Fig. 1(c)). The position and shape of the absorption peak are within the expected range, as a broad absorbtion peak between ≈ 900nm to 1300nm has been described for mixtures of CNTs and amorphous carbon [12,43]., The single peaks at 1100nm are independent of the polycation molecular weight, CNT concentration and film thickness. With each additional BL deposited, the peak intensity increased, as did the background.

Fig. 4(a) shows the Vis-NIR-absorption spectra for the CNT/PDADMA films prepared with the heavy PDADMA ($M_{w,PDADMA}$ = 322kDa and c_{CNT} = 0.15mg/ml). For films with 8 BL a maximum absorbance of 0.2211 at 1100nm was achieved. The same maximum absorbance (of 0.2211) was observed for CNT/PDADMA films with the same CNT concentration (0.15mg/ml) but decreased PDADMA molecular weight (44.3kDa, cf. Fig. 4(c)). Thus, it appears that the change of the PDADMA molecular weight does not influence the adsorption of the CNTs. In contrast, if the CNT concentration is increased up to 0.25mg/ml, ($M_{w,PDADMA}$ = 322kDa), the absorbance for 8 BL increases up to 0.2775, which is shown in Fig. 4(b).

The results are quantified and summarized in Fig. 4(d). The absorbance at the peak wavelength increases linearly with the film thickness for all CNT/PDADMA films. The constant slope demonstrates that CNT amount deposited at each adsorption step is the same, but the exact value depends on the CNT concentration used.

Whereas the slope for CNT/PDADMA films prepared from c_{CNT} = 0.15mg/ml is within error independent of the molecular weight of PDADMA, $0.0057 \pm 3{\cdot}10^{-4}$ (to be exact: $0.0053 \pm 4{\cdot}10^{-4}$ for $M_{w,PDADMA}$ = 322kDa and $0.0061 \pm 2{\cdot}10^{-4}$ for $M_{w,PDADMA}$ = 44.3kDa) the slope for films prepared with an increased CNT concentration of 0.25mg/ml is halved ($0.0028 \pm 9{\cdot}10^{-5}$).

3.5. Surface topography

AFM was applied to study the arrangement of the CNTs and the surface morphology. Images of CNT/PDADMA films for N = 1, 4 and 8 BL with a PDADMA molecular weight of 322 kDa and a CNT concentration of 0.15 mg/ml are shown in Fig. 5(a) to (c). In all cases flatly adsorbed CNTs are observed. They are randomly oriented and form a network, which resembles fallen jackstraws. Single-/double-walled and also bundles of CNTs can be identified. When only one CNT/PDADMA BL is deposited, one recognizes isolated CNTs, with very few cross-overs. A film consisting of four CNT/PDADMA BL shows a network of CNTs. The network is even more pronounced when the film consists of eight bilayers, additionally an increased roughness can be observed.

By changing the molecular weight and CNT concentration no significant difference was observed (data not shown). In Fig. 5(d) the development of the film/air roughness σ_{RMS} is shown for 1, 4 and 8 BL of deposited CNT/PDADMA BL. Films consisting of one CNT/PDADMA BL have all the same σ_{RMS}. With increasing BL number, for all CNT/PDADMA films investigated a linear increase in roughness is found. CNT/PDADMA films built with a PDADMA molecular weight of 44.3kDa and a low CNT concentration (0.15mg/ml) showed the lowest increase, with a slope of σ_{RMS} (nm) = 0.89N ± 0.03. CNT/PDADMA films prepared with an increased carbon nanotube concentration (0.25mg/ml) have the lowest CNT content per nm-thickness according to NIR absorption (cf. Fig. 3(d)). For films prepared with a higher PDADMA molecular weight, the roughness shows a larger increase with each additional layer, independent of the CNT concentration ($\sigma_{RMS,\ 322kDa,\ 0.15mg/ml}$ (nm) = 1.51N +

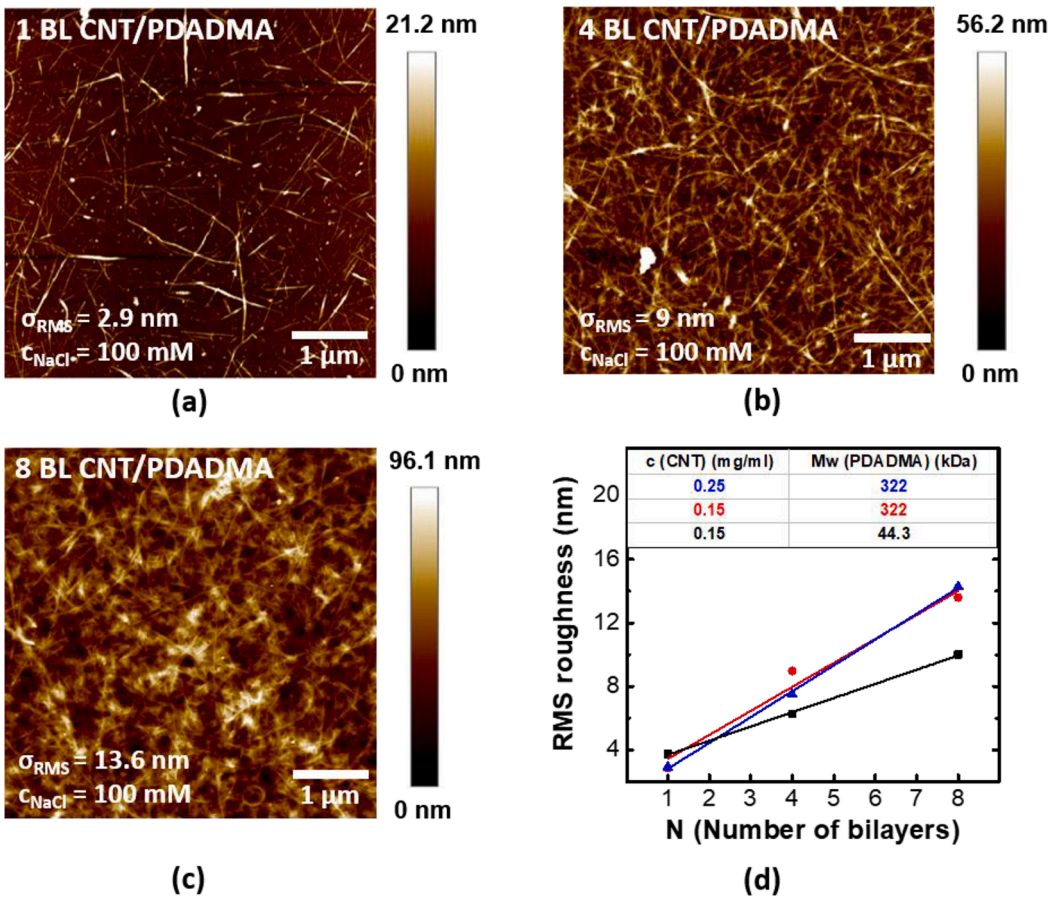

Fig. 5. AFM images ($5 \times 5\ \mu m^2$) in air of PEI/PSS/PDADMA/(CNT/PDADMA)$_N$ films, in dependence of N the number of CNT/PDADMA BL: **(a)** 1 BL, **(b)** 4 BL and **(c)** 8 BL ($M_{w,PDADMA} = 322$kDa, $c_{CNT} = 0.15$mg/ml. **(d)** RMS roughness in dependence of the number of depositedBL.

0.25 and $\sigma_{RMS,\ 322kDa,\ 0.25mg/ml}\ (nm) = 1.63N + 0.05$). Furthermore, all films were stable and homogeneous. The thickness of a CNT/PDADMA BL ((5.5 ± 0.5) nm for $c_{CNT} = 0.15$mg/ml and (16.5 ± 1.7) nm for $c_{CNT} = 0.25$mg/ml) exceeds the diameter of a carbon nanotube (1nm to 2nm). Since the AFM images show horizontal alignment of the CNTs, the thickness is presumably due to a single layer of CNTs covered by a polycation layer.

It is advantageous that the PDADMA were adsorbed from 0.1 M NaCl. At this ion concentration, PDADMA adsorbs in a coiled conformation which can be thicker than the diameter of the molecules (1 nm for PDADMA). Additionally, the NaCl ions in the deposition solution screen the electrical charges on the polycation chains, causing a low persistence length and allowing the PDADMA chains to adjust their conformation for optimum coverage of the CNTs. The variation of the parameters $M_{w,PDADMA}$ (44.3kDa and 322kDa) and CNT concentration in suspension (0.15mg/ml and 0.25mg/ml) showed that only changing the CNT concentration influenced the BL thickness (Δd_{BL}) of the films. The increase of c_{CNT} from 0.15mg/ml up to 0.25mg/ml results in an increase of Δd_{BL} by a factor of three (from $\Delta d_{BL} = 6$nm up to $\Delta d_{BL} = (17)$nm.). When the CNT concentration was kept constant (in adsorption suspension) and the PDADMA molecular weight was varied, we expected a similar influence on the thickness per deposited BL. However, we got exactly the same BL thickness ($\Delta d_{BL} = (5.5 \pm 0.5)$nm for $c_{CNT} = 0.15$mg/ml). The thickness of PDADMA monolayers depends on the selected deposition conditions on PDADMA molecular weight [18,39]. We conclude that the thickness of a CNT/PDADMA BL depends on the thickness of the CNT network only. PDADMA adsorbed onto CNTs provides a positively charged shell. Thick PDADMA monolayers were always observed on flat homogeneous substrates. CNTs do not provide these kinds of flat surfaces. Also, the absorption measurements show that the surface coverage per deposited CNT layer is independent of the PDADMA molecular weight. The only effect of the larger PDADMA molecular weight is the increase of the film/air roughness. The roughness is due to the CNT network. Each additional CNT layer adds more crisscrossing points; thus, the roughness increases. The thickness of the adsorption layer of the light PDADMA on flat surfaces is small [44], thus the increase in roughness is less pronounced. On increase of c_{CNT}, the thickness of a CNT/PDADMA BL gets thicker.

We assume that an increased CNT concentration leads to a fast adsorption process, without the possibility of the CNTs to rearrange. When in the next adsorption step PDADMA adsorbs on the disordered CNTs, the average thickness of the polymer layer is thick, thicker than on the low-coverage CNT layer. This leads to a factor three thicker CNT/PDADMA adsorption layer ($\Delta d_{BL} = (16.5 \pm 1.7)$nm for $c_{CNT} = 0.25$mg/ml). To understand this process further experiments are necessary in the future.

3.6. Electrical properties

The resistance of each film was measured using the set-up depicted in Scheme 1. For each film, the dependence between applied voltage and measured current could be described by Ohm's law (cf. Fig. 6(a)). As expected, with every additional CNT layer the sheet resistance decreases. The sheet resistance could be varied by one order of magnitude (factor 15), between ≈ 120 kΩ and ≈ 8 kΩ (data from 1 BL CNT/PDADMA and 8 BL CNT/PDADMA, respectively, $M_{w,PDADMA} = 322$ kDa, $c_{CNT} = 0.15$ mg/ml). Since the sheet resistance decreases inversely proportional to the film thickness d_{film}, the resistivity ρ is constant for a CNT/PDADMA system and was determined according to $\rho = R \cdot \frac{W \cdot d_{film}}{L}$,

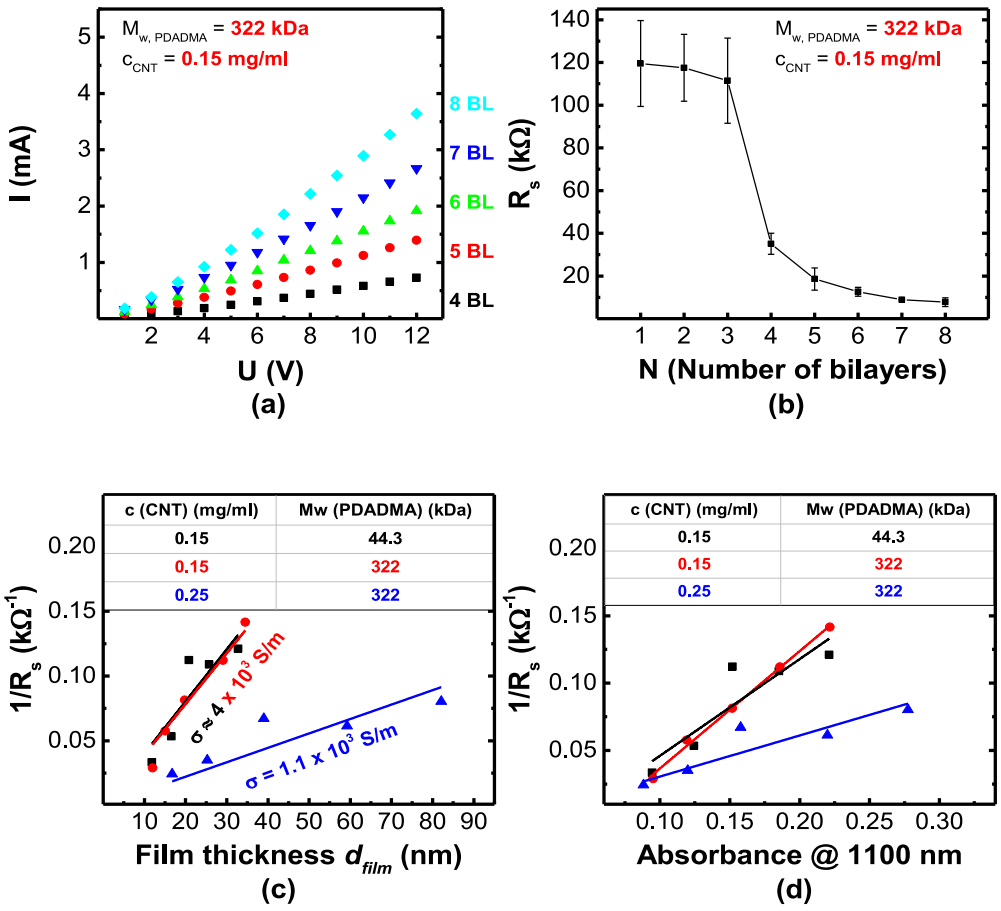

Fig. 6. Electrical properties of PEI/PSS/PDADMA/(CNT/PDADMA)$_N$ films consisting from N = 4 BL up to N = 8 BL. **(a)** Linear current I vs voltage U characteristics of a representative film prepared as indicated. All CNT/PDADMA films investigated exhibit ohmic behavior. From the slope the resistance was determined (5 kΩ to 20 kΩ). **(b)** Sheet resistance R_S in dependence of the number of deposited CNT/PDADMA BL ($M_{w,PDADMA}$ = 322kDa and c_{CNT} = 0.15mg/ml). Each R_S value shown is the average of three different films, error bars indicate the standard deviation. **(c)** The inverse sheet resistance increases linearly with the film thickness; from the slope of the linear fits the conductivity σ is determined. **(d)** The inverse sheet resistance increases linearly with the absorbance at 1100nm. Investigated were PEI/PSS/PDADMA/(CNT/PDADMA)$_N$ films, with N the number of CNT/PDADMA BL. All polyelectrolytes were adsorbed from a solution containing 0.1 M NaCl.

with film thickness d_{film} determined by ellipsometry. Fig. 6(b) also shows that four CNT/PDADMA BL are necessary to obtain a CNT network which is able to transport the electrons effectively through the film. Between three and four BL, the resistance drops by almost an order of magnitude. It looks like a percolation transition, after the deposition of four BL the lateral density of crossing points between CNTs is constant, and so is the conductivity. In dependence of the film composition, the measured conductivity varies by a factor of four.

The lowest conductivity $\sigma = \frac{1}{\rho} = 1.11 \cdot 10^3$ S/m was obtained for the CNT/PDADMA films with c_{CNT} = 0.25mg/ml, whereas films built with c_{CNT} = 0.15mg/ml had four times higher conductivity ($\approx 3.97 \cdot 10^3$ S/m). This conductivity ($\approx 3.97 \cdot 10^3$ S/m) is the largest that has been achieved in polyelectrolyte multilayers. But it is still two orders of magnitude smaller than that of films of pure CNTs [45].

Our results are consistent with the initial hypothesis: Charge transport from one CNT to the next is the main source of resistance. Since the CNTs are the conducting elements in the film we compare also the inverse sheet resistance with the optical absorbance at 1100nm (cf. Fig. 6 (d)). The dependence is linear, which is expected, since both the inverse of R_S and the film thickness increase linearly with the absorbance at 1100nm. It is remarkable that both the CNT coverage per layer and the conductivity are independent of the molecular weight of PDADMA and identical. This observation suggests that the scaffold formed by the CNTs determines the positions where PDADMA adsorbs, whereas the polymer length has no influence on scaffold formation.

Surprisingly, the CNT concentration in the deposition suspension has an influence, not only on the film thickness but also on the electrical conductivity. Panel (a) of Fig. 7 shows the linear growth region of CNT/PDADMA multilayers. The thickness increase per deposited CNT/PDADMA bilayer is three times larger when the CNTs are adsorbed from a more concentrated suspension. But for the thicker films, the increase in absorbance at 1100nm is only slightly larger than for the thinner films (see panel b of Fig. 7), so the CNT content in the thicker bilayers is only slightly increased. Therefore, the increased thickness of the CNT/PDADMA bilayers is caused by additional PDADMA content. Thus, the film composition is changed, the ratio PDADMA monomers/CNT is increased. The lower CNT content in the film leads to fewer crossing points of CNT rods, less charge transfer and thus increase in the sheet resistance and a concommitant decrease in the conductivity, as shown in panel (c) of Fig. 7.

We can only speculate why the increased CNT concentration in the suspension led to a larger thickness of the PDADMA adsorption layer in each adsorptin step. The increased thickness of the PDADMA adsorption layer indicates that the CNT conformation at the surface is different. We suggest that the increased concentration in the deposition suspension led to more tilted CNT rods, providing more adsorption sites for the PDADMA molecules. However, the changes have to be very subtle because we did not observe any differences in the AFM images of the films prepared from the different CNT suspensions. In summary, the higher the monomer/CNT ratio, the lower the conductivity is, as shown in Fig. 7.

4. Conclusions

With the aim of fabricating ultrathin electrically conductive layers for biological applications [46], multilayers of different PDADMA molecular weights and CNT concentrations were built using the LbL assembly method. Films were prepared by sequential adsorption of oxidized CNTs (from water) and PDADMA (from 0.1 M NaCl solution). The sheet resistance was highest for one CNT/PDADMA BL, and decreased monotonously with each added CNT/PDADMA BL. The electrical conductivity increased during the depositon of the first four

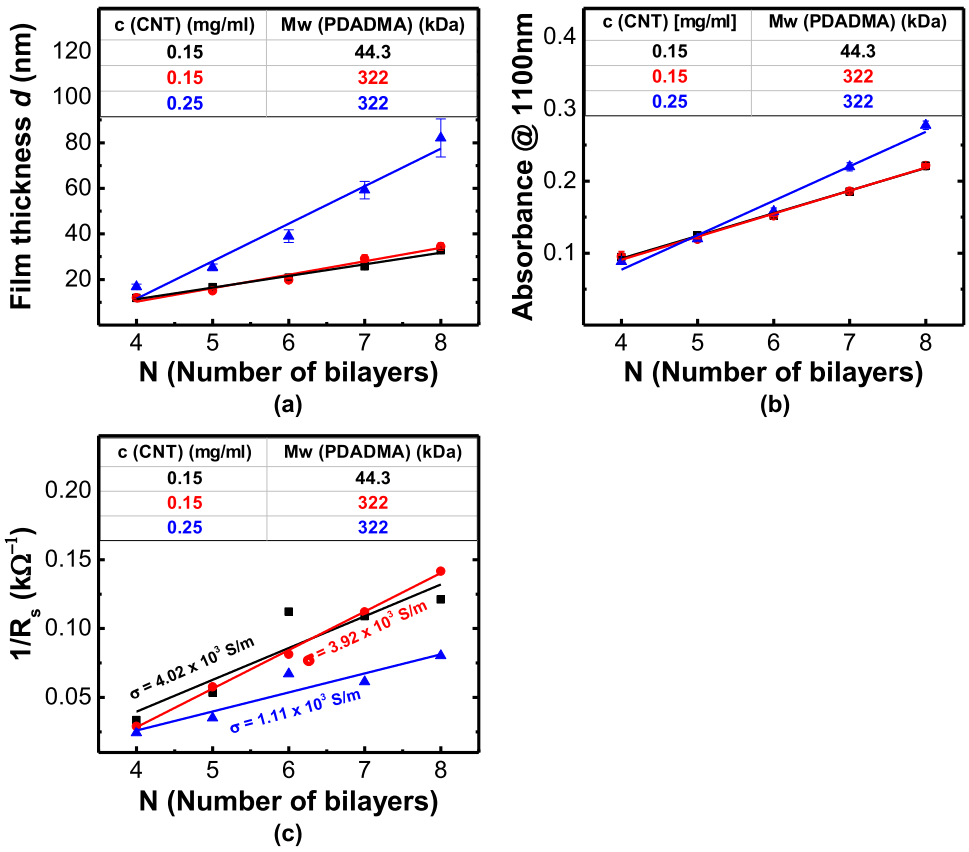

Fig. 7. PEI/PSS/PDADMA/(CNT/PDADMA)$_N$ films, where N denotes the number of CNT/PDADMA bilayers. The molecular weight of the polycation PDADMA and the concentration of the CNTs in the adsorption solution were varied as indicated. **(a)** Film thickness as a function of the number of BL measured by ellipsometry. **(b)** Dependence of absorbance at 1100nm and **(c)** inverse sheet resistance $1/R_S$ on the number of bilayers N.

CNT/PDADMA BL, then it was constant. This finding suggests that four CNT/PDADMA BL are necessary to obtain a constant coverage of CNT crossing points or nodes. With more than four CNT/PDADMA BL the sheet resistance depends only on the number of deposited BL. In our experiments, the sheet resistance could be varied by a factor of six, in dependence of the number of CNT/PDADMA BL. The thickness of each CNT/PDADMA BL was constant, as determined ellipsometrically [47]. Furthermore, the molecular weight of PDADMA was varied, by almost an order of magnitude. Even though the thickness of one adsorbed PDADMA monolayer depends on the molecular weight [2,39], the PDADMA molecular weight did not affect the thickness of a CNT/PDADMA BL, nor the electrical conductivity. We conclude that the polycations adsorb to the CNTs and the shape of the CNT network determines the thickness of a CNT/PDADMA BL, not the PDADMA molecular weight.

Two different CNT concentrations were used in the absorption suspension. A higher CNT concentration in the suspension correlated with an increased film thickness. It is suggested that the fast adsorption process of the CNTs led to more adsorption sites for the polycation. The lower CNT coverage per nm thickness increase (by a factor two) demonstrated that the ratio PDADMA monomer/CNT was increased, which led to a lower electrical conductivity.

AFM images of one CNT/PDADMA BL showed isolated CNTs, while AFM images of four or more BL showed flatly absorbed CNTs that lay crisscross on top of each other. They form a flat network, with many crossing points or nodes, which make electron transfer between CNTs possible. A percolation transition occurs when four BL are deposited, leading to the highest electrical conductivity reported so far for LbL films made with CNTs ($\approx$ 4000 S/m) was achieved.

Author contributions

S.N. oxidized the CNTs, built the multilayers and characterized them. He also performed the statistical analysis of the data. K.F. performed the XPS measurements and analyzed them. A.S. planned the chemical modification of the CNTs and validated it . P.N. analyzed the ellipsometric data. I.E. performed ellipsometric measurements. CAH planned the experiments. S.N., A.S., and C.A.H. wrote the manuscript, and all authors read and approved it.

Declaration of Competing interest

The authors declare that they have no known competing financial interests or personal relationships that could have appeared to influence the work reported in this paper.

Acknowledgement

We are grateful for the financial support of the German Research Foundation (DFG) Collaborative Research centre (CRC) ELAINE 1270 (SFB 1270/1 - 299150580). We want to thank the group of Prof. Dr. Sabine Müller for using their chemical laboratories and the group of Prof. Dr. Carola Schulzke (both from the University of Greifswald, Institute of Biochemistry, Greifswald, Germany). We want to thank especially Dr. Bettina Appel for her help.

References

[1] E. Gongadze, D. Kabaso, S. Bauer, T. Slivnik, P. Schmuki, U. van Rienen, A. Iglic, Adhesion of osteoblasts to a nanorough titanium implant surface, Int. J. Nanomed. 6 (2011) 1801–1816.

[2] A.R. Farooqi, J. Zimmermann, R. Bader, U. van Rienen, Numerical simulation of electroactive hydrogels for cartilage-tissue engineering, Materials (Basel) 12 (2019) 18.
[3] Y. Hanein, L. Bareket-Keren, Carbon nanotube-based multi electrode arrays for neuronal interfacing: progress and prospects, Front. Neural. Circ. 6 (2013) 122.
[4] L. Inzelberg, Y. Hanein, Electrophysiology meets printed electronics: the beginning of a beautiful friendship, Front. Neurosci. 12 (2019) 992.
[5] M.A. Sousa, J.R. Siqueira, A. Vercik, M.J. Schöning, O.N. Oliveira, Determining the optimized layer-by-layer film architecture with dendrimer/carbon nanotubes for field-effect sensors, IEEE Sens. J. 17 (2017) 1735–1740.
[6] P.V. Morais, V.F. Gomes, A.C. Silva, N.O. Dantas, M.J. Schöning, J.R. Siqueira, Nanofilm of ZnO nanocrystals/carbon nanotubes as biocompatible layer for enzymatic biosensors in capacitive field-effect devices, J. Mater. Sci. 52 (2017) 12314–12325.
[7] V.O. Fávero, D.A. Oliveira, J.L. Lutkenhaus, J.R. Siqueira, Layer-by-layer nanostructured supercapacitor electrodes consisting of ZnO nanoparticles and multi-walled carbon nanotubes, J. Mater. Sci. 53 (2018) 6719–6728.
[8] G. Decher, Fuzzy nanoassemblies: toward layered polymeric multicomposites, Science 277 (1997) 1232–1237.
[9] L. Fernández-Peña, E. Guzmán, F. Ortega, L. Bureau, F. Leonforte, D. Velasco, R. G. Rubio, G.S. Luengo, Physico-chemical study of polymer mixtures formed by a polycation and a zwitterionic copolymer in aqueous solution and upon adsorption onto negatively charged surfaces, Polymer (Guildf) 217 (2021), 123442.
[10] J. de Grooth, B. Haakmeester, C. Wever, J. Potreck, W.M. de Vos, K. Nijmeijer, Long term physical and chemical stability of polyelectrolyte multilayer membranes, J. Memb. Sci. 489 (2015) 153–159.
[11] W. Cheng, C. Liu, T. Tong, R. Epsztein, M. Sun, R. Verduzco, J. Ma, M. Elimelech, Selective removal of divalent cations by polyelectrolyte multilayer nanofiltration membrane: role of polyelectrolyte charge, ion size, and ionic strength, J. Memb. Sci. 559 (2018) 98–106.
[12] A.A. Green, M.C. Hersam, Processing and properties of highly enriched double-wall carbon nanotubes, Nat. Nanotechnol. 4 (2009) 64.
[13] N.W.S. Kam, E. Jan, N.A. Kotov, Electrical stimulation of neural stem cells mediated by humanized carbon nanotube composite made with extracellular matrix protein, Nano Lett. 9 (2009) 273–278.
[14] T.W. Ebbesen, Wetting, filling and decorating carbon nanotubes, J. Phys. Chem. Solids 57 (1996) 951–955.
[15] Z. Wu, Z. Chen, X. Du, J.M. Logan, J. Sippel, M. Nikolou, K. Kamaras, J. R. Reynolds, D.B. Tanner, A.F. Hebard, Transparent, conductive carbon nanotube films, Science 305 (2004) 1273–1276.
[16] M. Gu, W.-J. Song, J. Hong, S.Y. Kim, T.J. Shin, N.A. Kotov, S. Park, B.-S. Kim, Stretchable batteries with gradient multilayer conductors, Sci. Adv. 5 (2019) eaaw1879.
[17] Y. Akgöl, C. Cramer, C. Hofmann, Y. Karatas, H.-D. Wiemhöfer, M. Schönhoff, Humidity-dependent DC conductivity of polyelectrolyte multilayers: protons or other small ions as charge carriers? Macromolecules 43 (2010) 7282–7287.
[18] B.S. Shim, Z. Tang, M.P. Morabito, A. Agarwal, H. Hong, N.A. Kotov, Integration of conductivity, transparency, and mechanical strength into highly homogeneous layer-by-layer composites of single-walled carbon nanotubes for optoelectronics, Chem. Mater. 19 (2007) 5467–5474.
[19] A.R. Farooqi, J. Zimmermann, R. Bader, U. van Rienen, Numerical simulation of electroactive hydrogels for cartilage–tissue engineering, Materials (Basel) 12 (2019) 2913.
[20] S.W. Lee, B.S. Kim, S. Chen, Y. Shao-Horn, P.T. Hammond, Layer-by-layer assembly of all carbon nanotube ultrathin films for electrochemical applications, J. Am. Chem. Soc. 131 (2009) 671–679.
[21] P. Nestler, M. Paßvogel, C.A. Helm, Influence of polymer molecular weight on the parabolic and linear growth regime of PDADMAC/PSS multilayers, Macromolecules 46 (2013) 5622–5629.
[22] A. López-Oyama, R. Silva-Molina, J. Ruíz-García, R. Gámez-Corrales, R. Guirado-López, Structure, electronic properties, and aggregation behavior of hydroxylated carbon nanotubes, J. Chem. Phys. 141 (2014), 174703.
[23] K.A. Wepasnick, B.A. Smith, K.E. Schrote, H.K. Wilson, S.R. Diegelmann, D. H. Fairbrother, Surface and structural characterization of multi-walled carbon nanotubes following different oxidative treatments, Carbon 49 (2011) 24–36.
[24] X. Li, J. Niu, J. Zhang, H. Li, Z. Liu, Labeling the defects of single-walled carbon nanotubes using titanium dioxide nanoparticles, J. Phys. Chem. B 107 (2003) 2453–2458.
[25] L. Yue, W. Li, F. Sun, L. Zhao, L. Xing, Highly hydroxylated carbon fibres as electrode materials of all-vanadium redox flow battery, Carbon 48 (2010) 3079–3090.
[26] W. Kern, The evolution of silicon wafer cleaning technology, J. Electrochem. Soc. 137 (1990) 1887–1892.
[27] G. Decher, M. Eckle, J. Schmitt, B. Struth, Layer-by-layer assembled multicomposite films, Curr. Opin. Colloid Interface Sci. 3 (1998) 32–39.
[28] R.M. Azzam, N.M. Bashara, S.S. Ballard, Ellipsometry and polarized light, Phys. Today 31 (1978) 72.
[29] P. Nestler, S. Block, C.A. Helm, Temperature-induced transition from odd–even to even–odd effect in polyelectrolyte multilayers due to interpolyelectrolyte interactions, J. Phys. Chem. B 116 (2012) 1234–1243.
[30] S. Runde, H. Ahrens, F. Lawrenz, A. Sebastian, S. Block, C.A. Helm, Stable 2D conductive Ga/Ga (OxHy) multilayers with controlled nanoscale thickness prepared from gallium droplets with oxide skin, Adv. Mater. Interfaces 5 (2018), 1800323.
[31] J.G. Webster, Electrical Measurement, Signal Processing, and Displays, CRC Press, 2003.
[32] J.C. Vickerman, I.S. Gilmore, Surface Analysis: The Principal Techniques, John Wiley & Sons, 2011.
[33] C. Cushman, S. Chatterjee, G.H. Major, N. Smith, A. Roberts, M. Linford, Trends in advanced XPS instrumentation. 1. Overview of the technique, automation, high sensitivity, imaging, snapshot spectroscopy, gas cluster ion beams, and multiple analytical techniques on the instrument, Vac. Technol. Coat. (2016) 1–9.
[34] L. Stobinski, B. Lesiak, A. Malolepszy, M. Mazurkiewicz, B. Mierzwa, J. Zemek, P. Jiricek, I. Bieloshapka, Graphene oxide and reduced graphene oxide studied by the XRD, TEM and electron spectroscopy methods, J. Electron. Spectros Relat. Phenomena 195 (2014) 145–154.
[35] H. Estrade-Szwarckopf, XPS photoemission in carbonaceous materials: a “defect” peak beside the graphitic asymmetric peak, Carbon 42 (2004) 1713–1721.
[36] G. Moraitis, Z. Špitalský, F. Ravani, A. Siokou, C. Galiotis, Electrochemical oxidation of multi-wall carbon nanotubes, Carbon 49 (2011) 2702–2708.
[37] A. Theodosiou, B.F. Spencer, J. Counsell, A.N. Jones, An XPS/UPS study of the surface/near-surface bonding in nuclear grade graphites: a comparison of monatomic and cluster depth-profiling techniques, Appl. Surf. Sci. 508 (2020), 144764.
[38] V. Datsyuk, M. Kalyva, K. Papagelis, J. Parthenios, D. Tasis, A. Siokou, I. Kallitsis, C. Galiotis, Chemical oxidation of multiwalled carbon nanotubes, Carbon 46 (2008) 833–840.
[39] H. Ago, T. Kugler, F. Cacialli, W.R. Salaneck, M.S. Shaffer, A.H. Windle, R. H. Friend, Work functions and surface functional groups of multiwall carbon nanotubes, J. Phys. Chem. B 103 (1999) 8116–8121.
[40] V. Datsyuk, C. Guerret-Piécourt, J.-.C. Dupin, E. Flahaut, A. Peigney, C. Laurent, Double walled carbon nanotube/polymer composites via in-situ nitroxide mediated polymerisation of amphiphilic block copolymers, (2004).
[41] N. Zhang, J. Xie, V.K. Varadan, Functionalization of carbon nanotubes by potassium permanganate assisted with phase transfer catalyst, Smart Mater. Struct. 11 (2002) 962.
[42] R. Lobo, M. Pereira-da-Silva, M. Raposo, R. Faria, O. Oliveira Jr., In situ thickness measurements of ultra-thin multilayer polymer films by atomic force microscopy, Nanotechnology 10 (1999) 389.
[43] A. Ryabenko, T. Dorofeeva, G. Zvereva, UV–VIS–NIR spectroscopy study of sensitivity of single-wall carbon nanotubes to chemical processing and Van-der-Waals SWNT/SWNT interaction. Verification of the SWNT content measurements by absorption spectroscopy, Carbon 42 (2004) 1523–1535.
[44] M. Porus, P. Maroni, M. Borkovec, Structure of adsorbed polyelectrolyte monolayers investigated by combining optical reflectometry and piezoelectric techniques, Langmuir 28 (2012) 5642–5651.
[45] S.W. Lee, B.-.S. Kim, S. Chen, Y. Shao-Horn, P.T. Hammond, Layer-by-layer assembly of all carbon nanotube ultrathin films for electrochemical applications, J. Am. Chem. Soc. 131 (2009) 671–679.
[46] N.A. Kotov, J.O. Winter, I.P. Clements, E. Jan, B.P. Timko, S. Campidelli, S. Pathak, A. Mazzatenta, C.M. Lieber, M. Prato, Nanomaterials for neural interfaces, Adv. Mater. 21 (2009) 3970–4004.
[47] P Nestler, C.A. Helm, Determination of refractive index and layer thickness of nm-thin films via ellipsometry, Optics Express 25 (22) (2017) 27077–27085.